Preparation of Dendritic Copper Nanostructures and Their Characterization for Electroreduction

Ri Qiu,[†] Hyun Gil Cha,[§] Hui Bog Noh,[‡] Yoon Bo Shim,[‡] Xiao Li Zhang,[†] Ru Qiao,[†] Dun Zhang,[||] Yeong Il Kim,[†] Umapada Pal,[§] and Young Soo Kang*[,§]

Department of Chemistry, Pukyong National University, 599-1 Daeyeon-3-dong, Namgu, Busan 608-737, Korea, Department of Chemistry and Center for Innovative BioPhysio Sensor Technology, Pusan National University, Busan 609-735, Korea, Department of Chemistry, Sogang University, Seoul 121-742, Korea, Institute of Oceanology, Chinese Academic of Sciences, 7 Nanhai Road, Qingdao 266071, China

Received: May 6, 2009; Revised Manuscript Received: July 15, 2009

Dendritic copper nanostructures of different morphologies were synthesized by a surfactant-free electrochemical method. Single crystal nature of the nanostructures was revealed from their X-ray diffraction and electron diffraction patterns. Mechanism of dendrite formation was discussed from thermodynamic aspects using the concept of supersaturation. Supersaturation of the copper metal reduced on the surface of the electrode was the crucial factor for the generation of different morphologies. Effects of applied potential, temperature, and the solution concentration on the supersaturation were studied. The NO_3^- and H_2O_2 electroreduction ability of the dendritic materials was tested. Use of copper dendrite-modified electrode as NO_3^- sensor was demonstrated.

Introduction

Group IB metals such as Cu, Ag, and Au are important for heterogeneous catalytic applications. In particular, the catalytic properties of nanostructured metals have been the subject of considerable research.[1−3] Among these metals, the price of copper is lower than other noble metals, making copper one of the most promising catalysts for applications in large amounts. Copper-based nanomaterials have been applied in the electrocatalytic reduction of nitrite and nitric oxide[4] in methanol formation from gas (H_2/CO)[5] and other electroanalytical applications.[6−8]

A dendrite has a hierarchical structure consisting of a main stem and many side branches.[9] Dendritic materials have attracted much attention both for fundamental studies and for potential applications in catalysis and other fields.[10−19] Formation of dendritic structures of group IB metals was reported earlier.[15−19] Synthesis methods used in those studies include electroless deposition, electrodeposition, and solution-phase synthesis. Specifically, Liu et al. prepared Cu dendrites by electrodeposition,[18] in constant current mode applying current density as high as 3 A cm^{-2}. Syntheses of porous dendritic materials were reported by Paul et al. and Choi et al.[19] They demonstrated the formation of dendritic Cu fibers at relatively high applied potentials (1.5−12.0 V) in electrochemical process. During the fiber growth process, electrochemical actuation phenomena could be observed. However, the potential of those dendritic Cu nanostructures in electrocatalytic applications has not been studied enough.[20,21]

Since Cu catalyzes many different reactions, it is a convenient material to use in electrochemical reactions, as it can simply be electrodeposited directly on the surface of an electrode. No further chemical treatment or special technique is needed to affix the catalyst onto the electrode surface. The dendrite assembly is particularly used for heterogeneous catalysis because of its high surface area.

In our previous work, we described electrooxidation and detection of glucose on the basis of dendritic CuNi materials.[14] We showed that the CuNi alloy dendrites are effective in the glucose electrooxidation and detection in aqueous solutions. Herein, we describe an electrochemical method to obtain dendritic Cu nanostructures. The dendrites were obtained with the chronoamperometry technique from an aqueous solution without addition of any surfactant. Dendrite growth mechanism was described using thermodynamic principles. Influence of different parameters (temperature, working electrode potential, and solution concentration) on the supersaturation and morphologies of the resulting Cu nanostructures was studied. The NO_3^- and H_2O_2 electroreduction ability of the materials was studied. A NO_3^- sensor based on dendritic Cu nanostructure was fabricated and tested in the aqueous solution. Our results indicate that the dendritic Cu nanostructures are promising materials for NO_3^- and H_2O_2 reduction, as well as for fabricating NO_3^- sensor.

Experimental Section

Preparation and Characterization of Cu Structures. The electrodeposition of Cu was performed in a three-electrode cell using an EG&G potentiostat/galvanostat M263 A instrument. Cu foil (Aldrich, 99.98%) was used as the substrate for the electrodeposition. The foil was scratched by the sand paper and cleaned with deionized water (>18 MΩ cm, Nanopure Ultrapure water system). The area of the electrode dipped into the electrolyte solution was 0.4 cm^2. A coiled Pt wire electrode was used as the counter electrode, and a saturated calomel electrode (SCE) was used as reference electrode. All the potentials reported in this work are quoted with SCE as the reference electrode unless otherwise specified. The distance between the working and counter electrodes was 2.0 cm. A 10-mL mixture

* To whom correspondence should be addressed. E-mail: yskang@sogang.ac.kr.
[†] Pukyong National University.
[§] Sogang University.
[‡] Pusan National University.
[||] Chinese Academic of Sciences.

10.1021/jp904222b CCC: $40.75
Published on Web 08/14/2009

solution containing 0.1 M $CuCl_2$ (Aldrich, 99+%) and 0.1 M Na_2SO_4 (Shinyo Pure Chemicals, G.R. reagent) was added into cell for the electrolysis.

Chronoamperometry was applied to obtain the deposits from the mixture solution using different potentials (e.g., −0.2, −0.4, or −0.6 V). Electrodeposition was carried out in a stationary electrolyte solution without any stirring or protective gas bubbling. After 600 s of electrolysis, the electrode was taken out and washed with deionized water and acetone several times. Special care was taken when the electrode was removed from solution, so that the shear force between the solution and electrode surface did not break the dendrites.

X-ray diffraction (XRD, Philips, X'Pert-MPD System, Cu Kα radiation with $\lambda = 0.154056$ nm) was used to determine the metallic nature of the deposited Cu nanostructures. Electron diffraction (ED, JEOL, JEM-2010) was applied to analyze the crystal structure of the deposits at the edges of the dendrite. The morphologies of the samples were studied by a field-emission scanning electron microscope (FE-SEM, JEOL, JSM-6700F) and high-resolution transmission electron microscope (HRTEM, JEOL, JEM-2010). For HRTEM and ED, the deposits were removed from the electrode by ultrasonication for 15 min. XRD was carried out with the deposits scratched off from the electrode surface to avoid the influence of the Cu substrate.

Nitrate Ion Electroreduction Ability of Cu Dendritic Material. To test the nitrate ion electroreduction ability, the bare copper electrode and the copper electrodes modified by copper dendritic material were tested by the linear sweep voltammetric (LSV) technique. The electrodes modified with copper dendrites were obtained at potentials of −0.2, −0.4, −0.6, and −0.8 V with an electrolysis time of 600 s in a mixture solution containing 0.1 M Na_2SO_4 and 0.1 M $CuCl_2$. The electrode was placed in a three-electrode cell to characterize its electrochemical properties. A coiled Pt wire electrode and SCE were used as the counter electrode and reference electrode, respectively. The tip of the reference electrode was kept at the vicinity of the working electrode. A 10-mL aqueous solution containing 0.10 M Na_2SO_4 was added to the cell for the blank LSV test. The pH of the solution was adjusted to be 3.07 with the addition of HCl solution. After the reaction, the electrode was removed and washed by deionized water to clean the electrode surface. Later, the electrode was put into an 11-mL solution containing 0.1 M Na_2SO_4 and 0.01 M $NaNO_3$ (Katayama Chemical) to test its electroreduction ability to the nitrate ion. The LSV scanning rate was set to be 10 mV/s.

Cu Dendritic Material as a Sensor for NO_3^- Detection Based on Electrochemical Measurement. A Cu foil electrode modified by Cu dendrites was obtained by electrolysis using a potential of −0.6 V for 600 s. The area of the electrode dipped into the solution was 0.4 cm^2. After being washed by deionized water, the electrode was put into a 10-mL aqueous solution containing 0.10 M Na_2SO_4 as the electrolyte. The pH of the solution was adjusted to be 3.07 with the addition of HCl solution. The electrocatalytic reduction of NO_3^- [22] was performed on the Cu dendrite in an aqueous solution using LSV. The LSVs were recorded for Cu foil (Figure 8a,c) and electrochemically deposited Cu dendrite (Figure 8b,d) in a 0.1 M Na_2SO_4 + 0.1 M HCl solution. LSV curves (a) and (b) were recorded in a blank solution, and (c) and (d) after the addition of 1.0 mM NO_3^-, respectively. There were no reduction peaks in LSVs recorded for the Cu foil and Cu dendrite in a blank solution, while the electrocatalytic reduction peaks were observed in the LSVs recorded for Cu foil and Cu dendrite electrodes in a NO_3^- solution. With the addition of the NO_3^- into the blank electrolyte solution, a reduction peak (c) of a Cu foil was observed at −0.58 V and a small peak at −0.32 V, while an enhanced reduction peak (d) at about −0.46 V with a small side peak at −0.52 V and a small peak at around −0.27 V were observed for Cu dendrite. These redox peaks appeared at the potentials assigned as follows. The redox peak at −0.01 V corresponds to $Cu^{2+} \rightarrow Cu^+$. The peak at −0.27 V corresponds to $Cu^+ \rightarrow Cu$, and the peak at −0.46 V corresponds to $Cu^{2+} \rightarrow Cu$.[23,24] The small reduction peaks of the electrode in the nitrate-containing solution might have originated from different kinds of Cu(I) and Cu(II) ions species (CuO_2, Cu_2O_2, $CuNO_3$, etc.) formed on the Cu metal surface during the experiment. As shown in the inset (a′−d′) of Figure S1 in the Supporting Information, the reduction current peak of NO_3^- ions at Cu dendrite electrode increased on increasing the concentration of nitrate ions ((a′) 0.0, (b′) 0.1, (c′) 0.5, and (d′) 1.0 mM) in the electrolyte. The chronoamperometry technique was applied to electrolyze the solution and to measure the electrode response to different concentrations of NO_3^-. The potential was set at −0.5 V, and the electrolysis time was fixed at 1200 s. Different amounts of the solution containing $NaNO_3$ (0.11 M) and Na_2SO_4 (0.1 M) were added into the cell at the specific electrolysis times (Table 1) to monitor the electrode response to the different NO_3^- concentrations.

TABLE 1: Volume and Nitrate Concentration in Solution Containing $NaNO_3$ (0.11 M) and Na_2SO_4 (0.1 M) Added to the Cell for the Given Electrolysis Times

addition time (s)	solution amount (mL)	$[NO_3^-]$ in the cell (M)
120	0.02	2.2×10^{-4}
240	0.04	6.6×10^{-4}
360	0.08	1.5×10^{-3}
480	0.10	2.6×10^{-3}
600	0.20	4.6×10^{-3}
720	0.40	8.5×10^{-3}
840	0.80	1.5×10^{-2}
960	1.0	2.3×10^{-2}
1080	2.0	3.5×10^{-2}

Hydrogen Peroxide Electroreduction Ability of Cu Dendritic Material. To test the hydrogen peroxide electroreduction ability, the bare copper electrode and the copper electrodes modified by copper dendritic material were also tested by the LSV technique. Electrocatalytic reduction of H_2O_2 (30%, Junsei Chemical Co. G.R.) was also examined in an aqueous solution with LSV. LSVs were recorded for a Cu foil (Figure 10a,c) and Cu dendrite (Figure 10b,d) electrodes in 0.1 M Na_2SO_4 solution, with and without addition of 1.0 mM H_2O_2. Curves (a) and (b) were the LSVs recorded in a blank solution, and (c) and (d) after the addition of 1.0 mM H_2O_2, respectively. No reduction peak corresponding to the formation of Cu ion species on the electrode surface was observed for the (a) blank solution, Cu foil electrode, and Cu dendrite electrode. With the addition of H_2O_2 to the blank electrolyte solution, a catalytic reduction peak was observed (c) at −0.50 V for Cu foil, while an enhanced reduction peak (d) at about −0.47 V for the Cu dendrite was observed. As shown in the inset (a′−d′) of Figure 10, the catalytic peak current recorded for Cu dendrite electrode increased with increasing concentrations of H_2O_2 ((a′) 0.0, (b′) 0.1, (c′) 0.5, and (d′) 1.0 mM) in the electrolyte solution.

Results and Discussion

Figure 1 shows a typical HRTEM image of the Cu dendritic structure obtained using a potential of −1.0 V and an electrolysis time of 600 s. The image reveals a hierarchical structure formed

Figure 1. Typical HRTEM image of the dendritic Cu nanostructure. The sample was obtained at a potential of −1.0 V with an electrolysis time of 600 s in a 10-mL aqueous solution containing $CuCl_2$ (0.1 M) and Na_2SO_4 (0.1 M).

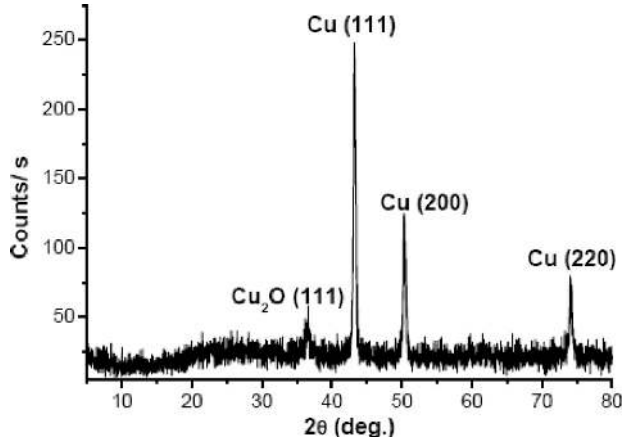

Figure 2. XRD pattern of a dendritic Cu nanostructure. The sample was obtained at a potential of −1.0 V with an electrolysis time of 600 s in a 10-mL aqueous solution containing $CuCl_2$ (0.1 M) and Na_2SO_4 (0.1 M).

during the electrolysis process. For the higher-order branches, the dimension can reach as small as a few nanometers. The ED pattern was obtained to confirm the single-crystal nature of the nanostructures. XRD pattern shown in Figure 2 confirms the metallic nature of the as-grown Cu nanostructures. The XRD peaks match well with the cubic phase of Cu (JCPDS 04-0836), with some residual Cu_2O (JCPDS 75-1531).

Figure 3 shows the FE-SEM images of the samples obtained at different electrolysis potentials at a fixed concentration (0.1 M) and temperature (23 °C). The FE-SEM images demonstrate that application of different potentials results in the different morphologies of Cu. During the electrolysis process, the applied potentials (−0.2, −0.4, −0.6, and −0.8 V) were sufficient for the reaction $Cu^{2+} + 2e = Cu$ ($E° = 0.339$ V vs SHE) to take place on the working electrode. For the materials obtained at lower potentials (−0.2 and −0.4 V), the dendritic structures were rarely observed. The morphologies shown in Figure 3a,b,

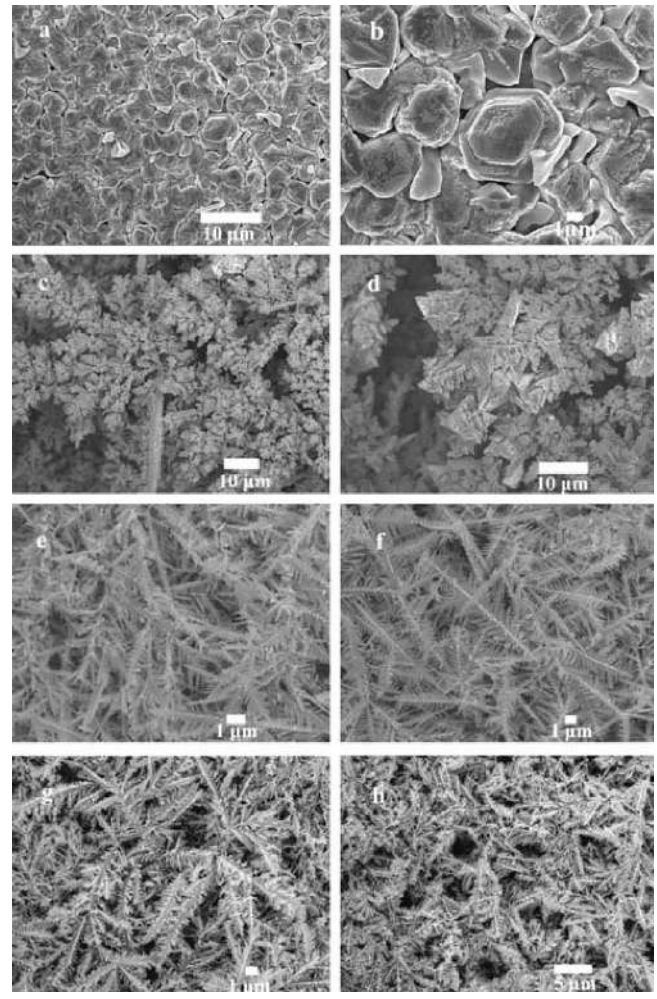

Figure 3. Typical FE-SEM images of Cu structures obtained at different potentials: (a, b) −0.2, (c, d) −0.4, (e, f) −0.6, and (g, h) −0.8 V. The electrolysis was carried out for 600 s at 23 °C.

for example, were obtained using −0.2 V. The deposit in this case seems to consist of discrete convex bumps. At the more negative potential of −0.4 V (Figure 3c,d), randomly branched crystal growth was observed. We expect that the fast growth rate observed at the higher potential causes the Cu to fill in the gaps between the initially deposited bumps. At yet higher potentials (−0.6, −0.8, and −1.0 V), dendritic structures were clearly observed. Typical morphologies of the Cu dendrites can be seen in Figure 3.

To study the effect of electrolysis time on the growth process, the nanostructures were grown at different electrolysis times for a fixed potential. The morphologies obtained with different electrolysis times at a potential of −0.6 V are shown in Figures 3e,f and 4. For the different electrolysis times, the morphologies are more or less similar, with certain differences. The material obtained with the shortest electrolysis time as shown in Figure 4a,c appears nonuniform and consists of smaller dendrites. For the longer electrolysis time, the dendrites are more uniform (Figures 3e,f and 4e,f), and the dendrite coverage on the electrode surface is high.

Variations of current with electrolysis time for different applied potentials are shown in Figure 5. As expected, the current increases during the electrolysis as the surface area of the copper increases. As the dendrites grow, branches develop at the apexes of crystals, which penetrate the diffusion layer to get the mass transfer to support the further growth. In other

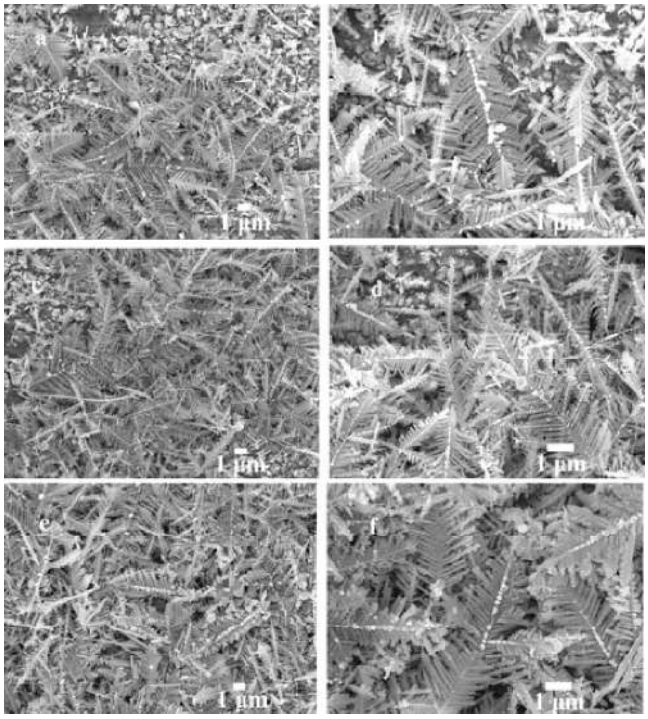

Figure 4. Typical FE-SEM images of Cu nanostructures obtained at a potential of −0.6 V with different electrolysis times: (a, b) 30, (c, d) 60, and (e, f) 120 s at 23 °C.

words, the surface area of the working electrode is continuously changing during the electrolysis process, as is the diffusion layer on the surface of the metal.

In general, if the H_2 evolution can be ignored during the electrolysis, the Cu crystal growth rate increases with the increase of current supplied to the working electrode. Therefore, we assume that the variation of current in the $I-t$ curves (Figure 5) indirectly reflects the variation of growth rate of the nanostructures. The crystal morphology changes depending on the growth rate. The relationship between growth rate (R) and the solution supersaturation ($\Delta\mu/kT$) was described in previous reports.[14,25] The supersaturation parameter is a characteristic parameter of the crystal growth from the solution phase. Here we refer to this parameter as $\Delta\mu/kT$, which has a direct positive relationship to the Cu crystal growth rate on the surface of the electrode. In our previous work on the study of supersaturation effect on the morphology of CuNi crystals, we varied only the working electrode potential. In the present work, we consider the additional parameters such as precursor ($CuCl_2$) concentration and the reaction temperature. Change in these parameters changes the current to the working electrode and hence the crystal growth rate. Different growth rates lead to different final morphologies of the Cu deposits. We propose that measuring the $I-t$ curves for a given sample allows us to predict morphology of the final product. Schematic illustrations of the predicted morphologies are shown to the right of the $I-t$ plots in Figure 5. At highly negative potential, larger precursor concentration, and high temperature, the supersaturation favors dendritic structure formation.

To describe the dynamics of the dendritic structure formation, we apply the classical crystal growth theory parallel grouping, shown schematically in Figure 6. The inner side of cubic Cu structure (Figure 7b) can also be observed, indicating that the deposition occurs more easily on the vertical angle of the cube. Repetition of this process eventually forms the dendritic structures.

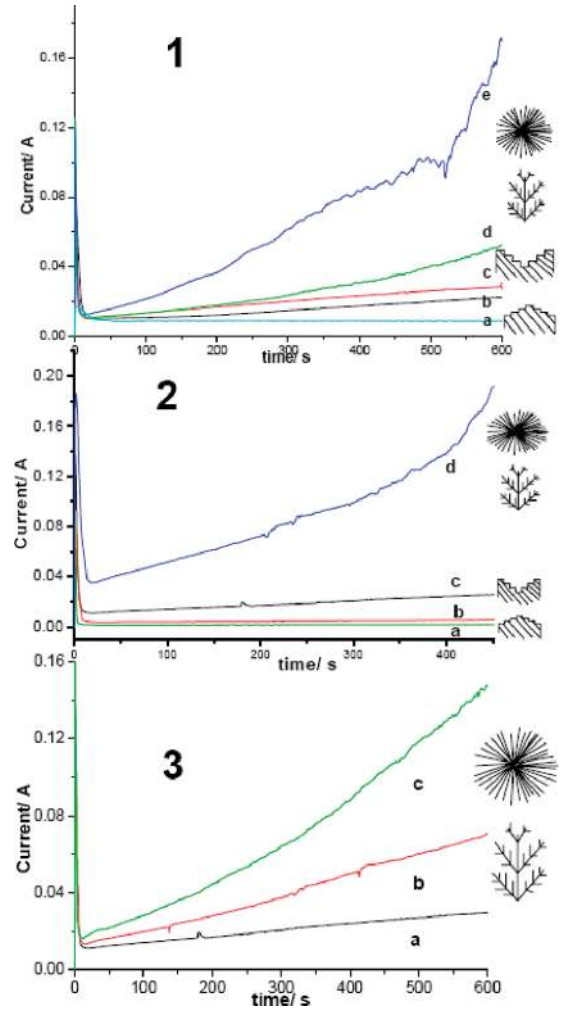

Figure 5. Chronoamperograms for electrolysis processes in 10-mL mixture of 0.1 M $CuCl_2$ and 0.1 M Na_2SO_4 solution (1) for different potentials (a) −0.2, (b) −0.4, (c) −0.6, (d) −0.8, and (e) −1.0 V; and (2) for different $CuCl_2$ concentrations at electrolysis potentials of −0.6 V: (a) 0.025, (b) 0.05, (c) 0.1, and (d) 0.2 M; and (3) at different temperatures (at fixed potential of −0.6 V): (a) 23, (b) 37, and (c) 51 °C. Proposed morphologies are shown to the right of each figure.

The relationship between working electrode potential and morphology of the deposits is clearly illustrated in the FE-SEM images shown in Figure 7. The images show that the bumps tend to form at lower potentials. Small cubic crystals are formed on the surface (Figure 7a,b). When we attempted to obtain an image of one of these cubes, the structure collapsed because of the melting of Cu nanostructures by the high electron energy of the FE-SEM. For higher potentials such as −0.4 V, cavities on the surface of the crystal can be observed (Figure 7d). We believe that these cavities are seed sites of the dendritic structures. If the crystal growth time is long enough, branches of the crystals grow, forming the dendrite structures (Figure 7c). If the potential is more negative (e.g. −0.8 V), the deposited metal grows with dendritic or whisker structures (Figure 7e,f).

To evaluate the Cu dendrite as an electrode material for practical application, we studied the NO_3^- and H_2O_2 electroreduction ability of a Cu dendrite-modified electrode in aqueous solution. For the NO_3^- detection, an electrochemical sensor based on the Cu dendrite-modified electrode was also fabricated.

NO_3^- reduction by electrochemical methods has attracted much attention because NO_3^- reduction in water solution is important for environmental remediation.[6−8,26−30] Copper is one

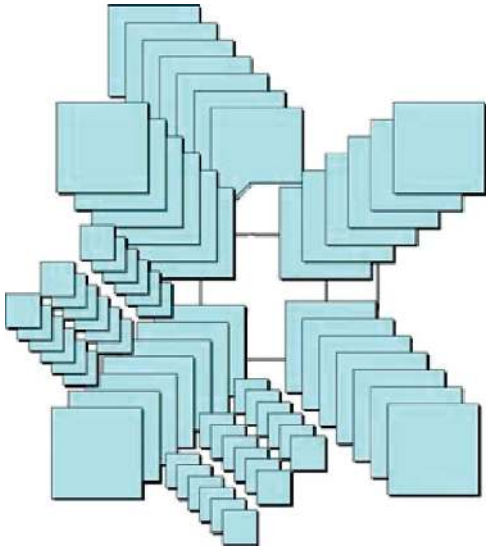

Figure 6. Schematic illustration of the dendrite structure formation process. The inner core is the primary cubic copper. Hierarchical structures grow over the primary structure as the growth process continues.

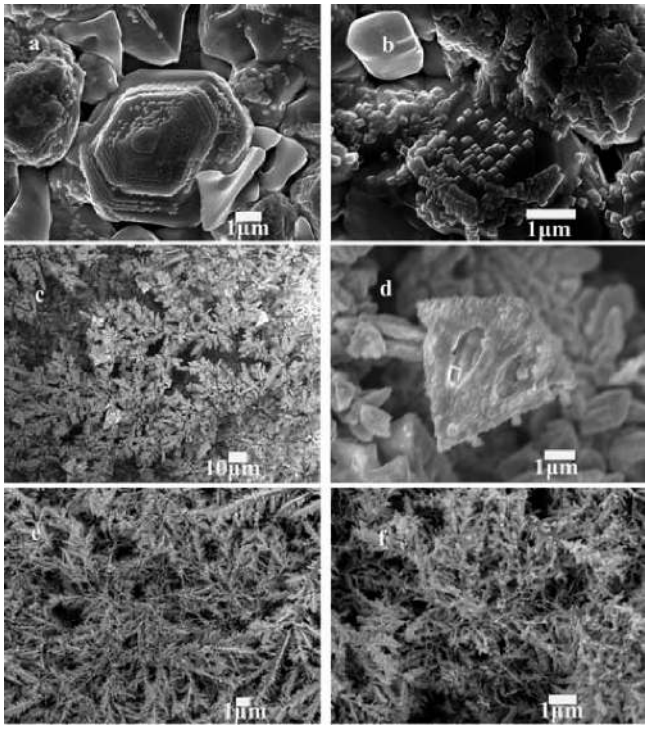

Figure 7. Typical FE-SEM images of the Cu nanostructures obtained at different potentials: (a, b) −0.2, (c, d) −0.4, and (e, f) −0.8 V. The electrolysis was carried out in a 10-mL electrolyte solution (containing 0.1 M $CuCl_2$ and 0.1 M Na_2SO_4) for 600 s, at 23 °C.

of the most effective metals to catalyze the reaction $NO_3^- + 8e^- + 9H^+ \rightarrow 3H_2O + NH_3$ in aqueous solution.[29] NO_3^- electroreduction ability was tested in aqueous solution using the LSV technique (see the Supporting Information for details). A comparison of current versus time curves between a blank solution of Na_2SO_4 (0.1 M) and a mixed solution of Na_2SO_4 (0.1 M) and $NaNO_3$ (0.01 M), both using the Cu dendrite-modified electrode, is shown in the inset of Figure 8. With the addition of NO_3^- to the blank solution, a peak appears near −0.45 V, which is attributed to the reduction peak of NO_3^-. A comparison of the NO_3^- electroreduction ability between Cu foil and copper dendrite-modified electrodes is shown in Figure

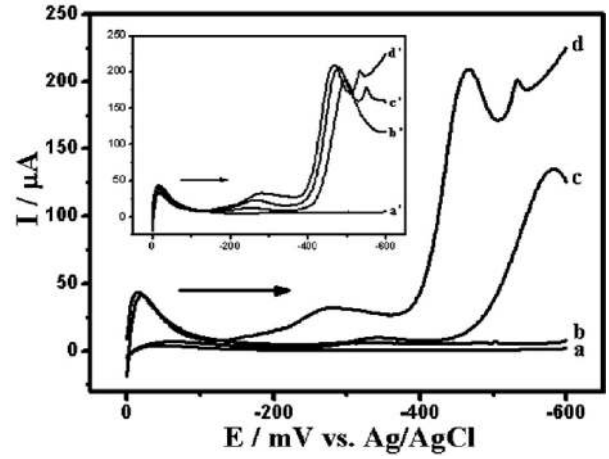

Figure 8. LSVs recorded for (a, c) a Cu foil and (b, d) Cu dendrite electrodes in a 0.1 M Na_2SO_4 + HCl solution at a scan rate of 10 mV/s. (a, b) For blank solution only; (c, d) for solution containing 1.0 mM $NaNO_3$. Inset: LSVs recorded for a Cu dendrite electrode at the different concentrations of NO_3^- ((a′) 0.0, (b′) 0.1, (c′) 0.5, and (d′) 1.0 mM) in a measuring solution.

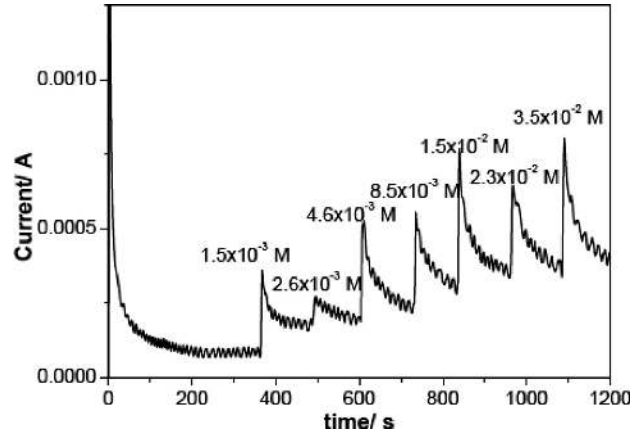

Figure 9. Chronoamperometry curve showing current versus time for NO_3^- detection. The electrode was modified with Cu dendrites obtained at −0.6 V for 600 s in a solution 0.1 M Na_2SO_4 and 0.1 M $CuCl_2$.

8. The modified electrodes were obtained at potentials of −0.2, −0.4, −0.6, and −0.8 V with electrolysis time of 600 s from $CuCl_2$ solution. From these LSV curves, we see that the electrodes modified at more negative potentials result in a larger peak current. We ascribe this result to the larger surface coverage of the dendrite-modified electrodes obtained at the higher potentials.

After confirming the NO_3^- electroreduction ability, NO_3^- detector was fabricated by using a Cu foil electrode modified by Cu dendrites in the aqueous solution. The electrode was modified at −0.6 V for 600 s in a 10-mL solution containing Na_2SO_4 (0.1 M) and $CuCl_2$ (0.1 M). Amperometry with the potential of −0.5 V was applied to check the electrode response to the different concentrations of NO_3^-. In Figure 9, the electrode response to the different concentrations of NO_3^- (electrolyte prepared with different amounts of $NaNO_3$) is shown. NO_3^- concentrations as low as 1.5×10^{-3} M could be detected by our Cu dendrite-modified sensor.

Fuel cells based on $NaBH_4/H_2O_2$ have attracted attention because of their many advantages compared to the traditional H_2/O_2 or methanol/O_2 fuel cells.[32,33] The electroreduction of H_2O_2 as the oxidant on the cathode is an important process for realizing this type of fuel cell. Finding an appropriate metal or

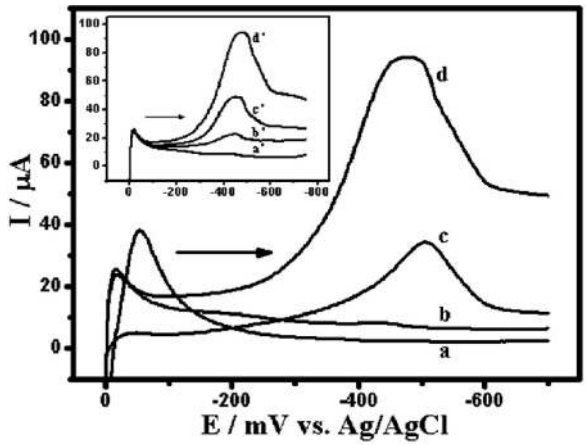

Figure 10. LSVs recorded for (a, c) Cu foil and (b, d) Cu dendrite electrodes in a 0.1 M Na_2SO_4 solution, at a scan rate of 10 mV/s. (a, b) For blank solution only; (c, d) for solution containing 1.0 mM H_2O_2. Inset: LSVs recorded for a Cu dendrite electrode at the different concentrations of H_2O_2 ((a′) 0.0, (b′) 0.1, (c′) 0.5, and (d′) 1.0 mM) in the measuring solution.

alloy to act as the cathode for the electrocatalysis of H_2O_2 is an important target. Previously, single-crystal Cu was investigated as the cathode.[34] Several researchers reported the electroreduction of H_2O_2 using Au and Fe.[35,36]

The LSV curves of Cu foil and copper dendrite-modified electrodes in H_2O_2 aqueous solution are shown in Figure 10. From the comparison (shown in the inset) between the blank solution of Na_2SO_4 and the mixed solution of Na_2SO_4 and H_2O_2, it is apparent that both using the Cu dendrite-modified electrode have the reduction functioning with different potentials (see the Supporting Information for details). The peak near −0.3 V is ascribed to the reduction of $HOO^\bullet$ through the reaction $HOO^\bullet + H^+ + e^- \rightarrow 2H_2O_2$, because $HOO^\bullet$ exists in the bulk solution (at the pH of the aqueous solution, ca. 5.60, the reaction $2H_2O_2 \rightarrow HOO^\bullet + H^+ + e^-$ is likely). From the LSV curves 1−4, it is clear that the peak currents are different. This is attributed to the differences in the surface area of the working electrode, as mentioned in the nitrate ion reduction results. When a more negative potential is applied to obtain Cu dendrites in larger surface area with the same electrolysis time, the larger surface area allows a more effective electroreduction, which is manifested in its reduction current peaks.

Conclusions

Dendritic Cu nanostructures could be obtained by the chronoamperometry technique. Electrolysis parameters such as bias potential, precursor concentration, and temperature determine the morphology of the resulting dendritic Cu nanostructures. At higher negative potential, larger precursor concentration, and high temperatures, the supersaturation favors the growth of dendritic structures. The high surface area dendritic nanostructures can be used for the electroreduction of NO_3^- and H_2O_2 and sensor for NO_3^- detection.

Acknowledgment. This work was supported by Korean Research Foundation Grant funded by the Korean government (MOEHRD) (KRF-2007-C00154). Special thanks are given to the financial support of Brain Korea 21 and the Nano R&D program of KOSEF.

Supporting Information Available: Additional LSVs of $NaNO_3$ and H_2O_2 electrocatalytic processes. This material is available free of charge via the Internet at http://pubs.acs.org.

References and Notes

(1) Min, B. K.; Friend, C. M. *Chem. Rev.* **2007**, *107*, 2709.
(2) Henglein, A. *Angew. Chem., Int. Ed.* **1979**, *18*, 418.
(3) Zhu, X.; Gan, X.; Wang, J.; Chen, T.; Li, G. *J. Mol. Catal. A: Chem.* **2005**, *239*, 201.
(4) Wang, H.; Huang, Y.; Tan, Z.; Hu, X. *Anal. Chim. Acta* **2004**, *526*, 13.
(5) Vukojević, S.; Trapp, O.; Grunwaldt, J. D.; Kiener, C.; Schüth, F. *Angew. Chem., Int. Ed.* **2005**, *44*, 7978.
(6) Davis, J.; Moorcroft, M. J.; Wilkins, S. J.; Compton, R. G.; Cardosi, M. F. *Analyst* **2000**, *125*, 737.
(7) Welch, C. M.; Hyde, M. E.; Banks, C. E.; Compton, R. G. *Anal. Sci.* **2005**, *21*, 1421.
(8) Davis, J.; Moorcroft, M. J.; Wilkins, S. J.; Compton, R. G.; Cardosi, M. F. *Electroanalysis* **2000**, *12*, 1363.
(9) Galenko, P. K.; Zhuravlev, V. A. *Physics of Dendrites: Computational Experiments*; World Scientific: Singapore, 1994.
(10) Matsushita, M.; Sano, M.; Hayakawa, Y.; Honjo, H.; Sawada, Y. *Phys. Rev. Lett.* **1984**, *53*, 286.
(11) Yan, H.; He, R.; Johnson, J.; Law, M.; Saykally, R. J.; Yang, P. *J. Am. Chem. Soc.* **2003**, *125*, 4728.
(12) Cao, M.; Liu, T.; Gao, S.; Sun, G.; Wu, X.; Hu, C.; Wang, Z. L. *Angew. Chem., Int. Ed.* **2005**, *44*, 4197.
(13) Shin, H.; Liu, M. *Adv. Funct. Mater.* **2005**, *15*, 582.
(14) Qiu, R.; Zhang, X. L.; Qiao, R.; Li, Y.; Kim, Y. I.; Kang, Y. S. *Chem. Mater.* **2007**, *19*, 4174.
(15) Fang, J.; Ma, X.; Cai, H.; Song, X.; Ding, B. *Nanotechnology* **2006**, *17*, 5841.
(16) Martin, H.; Carro, P.; Hernandez Creus, A.; Gonzalez, S.; Andreasen, G.; Salvarezza, R. C.; Arvia, A. J. *Langmuir* **2000**, *16*, 2915.
(17) Wen, X.; Xie, Y. T.; Mak, W. C.; Cheung, K. Y.; Li, X.-Y.; Renneberg, R.; Yang, S. *Langmuir* **2006**, *22*, 4836.
(18) Shin, H.; Dong, J.; Liu, M. *Adv. Mater.* **2003**, *15*, 1610.
(19) (a) Lopez, C. M.; Choi, K.-S. *Langmuir* **2006**, *22*, 10625. (b) Choi, K.-S. *Dalton Trans.* **2008**, *40*, 5432. (c) Siegfried, M. J.; Choi, K. S. *Angew. Chem., Int. Ed.* **2008**, *47*, 368. (d) Panda, B. R.; Rao, P. N.; Paul, A.; Chattopadhyay, A. *J. Phys. Chem. B* **2006**, *110*, 22917.
(20) Hu, C.; Gao, Z.; Yang, X. *J. Cryst. Growth* **2007**, *306*, 390.
(21) Wu, M.; Zhang, Q.; Liu, Y.; Fang, Q.; Liu, X. *Mater. Res. Bull.* **2009**, *44*, 1437.
(22) Shiddiky, M. J. A.; Won, M.-S.; Shim, Y.-B. *Electrophoresis* **2006**, *27*, 4545.
(23) Won, M.-S.; Park, J.-h.; Shim, Y.-B. *Electroanalysis* **1993**, *5*, 451.
(24) Bard, A. J. *Encyclopedia of Electrochemistry of the Elements*; M. Dekker: New York, 1973; Chapter II-6.
(25) Sunagawa, I. *Morphology of Crystals*; Kluwer Academic: Dordrecht, The Netherlands, 1987.
(26) Moorcroft, M. J.; Davis, J.; Compton, R. G. *Talanta* **2001**, *54*, 785.
(27) Reyter, D.; Chamoulaud, G.; Belanger, D.; Roue, L. *J. Electroanal. Chem.* **2006**, *596*, 13.
(28) Pletcher, D.; Poorabedi, Z. *Electrochim. Acta* **1979**, *24*, 1253.
(29) Carpenter, N. G.; Pletcher, D. *Anal. Chim. Acta* **1995**, *317*, 287.
(30) Bae, S. E.; Stewart, K. L.; Gewirth, A. A. *J. Am. Chem. Soc.* **2007**, *129*, 10171.
(31) Dima, G. E.; de Vooys, A. C. A.; Koper, M. T. M. *J. Electroanal. Chem.* **2003**, *554*, 15.
(32) Miley, G. H.; Luo, N.; Mather, J.; Burton, R.; Hawkins, G.; Gu, L.; Byrd, E.; Gimlin, R.; Shrestha, P. J.; Benavides, G.; Laystrom, J.; Carroll, D. *J. Power Sources* **2007**, *165*, 509.
(33) Gu, L.; Luo, N.; Miley, G. H. *J. Power Sources* **2007**, *173*, 77.
(34) Stewart, K. L.; Gewirth, A. A. *Langmuir* **2007**, *23*, 9911.
(35) Zhang, J.; Oyama, M. *J. Electroanal. Chem.* **2005**, *577*, 273.
(36) Guo, L.; Huang, Q. J.; Li, X.-Y.; Yang, S. *Langmuir* **2006**, *22*, 7867.

JP904222B